Highlights

A gray-box model for unitary air conditioners developed with symbolic regression

Shahzad Yousaf, Craig R. Bradshaw, Rushikesh Kamalapurkar, Omer San

- Development of a component-based gray-box model of a unitary air conditioner using symbolic regression
- Genetic algorithm used to formulate overall heat transfer coefficient correlation
- The model exhibits robustness and generalization, even with minimal training data
- Novel model utilizes only ambient temperatures and operational inputs, facilitating seamless integration into existing BEMs.

A gray-box model for unitary air conditioners developed with symbolic regression

Shahzad Yousaf[a,1,*], Craig R. Bradshaw[a], Rushikesh Kamalapurkar[b], Omer San[c]

[a] *Air Conditioning and Refrigeration Center, University of Illinois, Urbana-Champaign, IL, USA.*

[b] *Department of Mechanical and Aerospace Engineering, University of Florida, Gainesville, FL, USA.*

[c] *Department of Mechanical, Aerospace and Biomedical Engineering, University of Tennessee, Knoxville, TN, USA.*

Abstract

In this paper, we present the development of a gray-box model for unitary air conditioning equipment that can be trained with as little as 5 data points with higher accuracy on test data. The model utilizes the same model inputs as is typical in building energy simulation, and is accurate. While black-box models require large data sets to deliver accurate results, white-box models require higher computational and engineering efforts along with detailed knowledge of the system, and are often difficult to obtain. The model presented here addresses a hybrid solution that is a steady-state, component-based, gray-box model that requires inputs from the source and sink fluids and rated performance of the specific piece of equipment, only. The basic physics of a vapor compression cycle are captured in individual component models for the heat exchangers, compressor, and expansion valve. These components are generalized to eliminate refrigerant-side inputs. A key addition is the development of correlations for the overall heat transfer coefficient times surface area (UA) obtained from Symbolic Regression (SR). The model successfully predicts the cooling capacity, coefficient of performance (COP), and sensible heat ratio (SHR) for three state-of-the-art variable speed, split-system, air conditioning systems with capacities of 12.3(3.5), 14(4), and 17.6(5) kW(tons), achieving a mean absolute percentage error (MAPE) of less than 3.4%. These results suggest that the gray-box model can be useful in predicting the performance of similar systems in the future, which could be valuable for energy management and optimization purposes.

Keywords: Gray-box model, building energy modeling, symbolic regression, unitary air-conditioning system, energy performance gap

[*] Corresponding author,Tel: +1-(405)-894-0044

Email address: syousaf3@illinois.edu (Shahzad Yousaf)

Nomenclature

Variables

A	Area, (m^2)
c_p	Specific heat capacity, (kJ (kg K)$^{-1}$)
h	Enthalpy, (kJ kg^{-1})
h	Heat transfer coefficient, (Wm^{-2}K^{-1})
$\dot{m}$	Mass flow rate, (kg s^{-1})
P	Pressure, (kPa)
$\dot{Q}$	Heat flow capacity, (kW)
T	Temperature, (K)
UA	Overall heat transfer ratio times area, (W K^{-1})
$\dot{V}$	Volumetric air flow rate, (m^{3}s^{-1})
$\dot{W}$	Power, (kW)

Subscripts

a	Air
act	Actual
adp	Apparatus dew point
ca	Condenser air
$comp$	Compressor
$cond$	Condenser
ea	Evaporator air
$evap$	Evaporator
idt	Indoor dry-bulb
is	Isentropic
iwb	Indoor wet-bulb
Net	Net
odt	Outdoor dry-bulb
rat	Rated
ref	Refrigerant
s	Evaporator surface
$suct$	Suction
sup	Supply
$temp$	Temperature

Acronyms

AHRI	Air-conditioning, heating, and refrigeration
BEM	Building energy model
BF	Bypass factor
CFM	Cubic feet per minute
COP	Coefficient of performance
EPG	Energy performance gap
HEX	Heat exchanger
HVAC	Heating ventilation air conditioning
MAPE	Mean absolute percentage error
MB	Moving boundary
ML	Machine learning
NTU	Number of transfer units
RMSE	Root mean square error
SC	Sub cooling
SH	Superheat
SHR	Sensible heat ratio
SR	Symbolic regression
VCS	Vapor compression system

Constants

α_0, α_1	Regression coefficients
$\beta_0, \beta_1, \beta_2$	Regression coefficients
a_0, a_1, a_2	Regression coefficients
c_0, c_1, c_2	Regression coefficients
$e_0, e_1, .., c_{10}$	Compressor map coefficients
n	Number of data points

Greek Symbols

Δ	Difference (e.g., enthalpy difference)
ε	Effectiveness, (-)
ν	Specific volume, (m^3.kg^{-1})
ϕ	Relative humidity, (%)
ψ	Humidity ratio, (-)

1. Introduction

Understanding building energy usage is necessary for maximizing energy use and grid flexibility. In 2020, total building energy used in the United States amounted to 20 quadrillion British thermal units (BTU), of which more than 50% is used in heating, ventilation, and air conditioning (HVAC) applications AEO (2020). Therefore, HVAC systems and appliances are of paramount importance to reduce overall building energy utilization. Emphasis on models with reliable model predictive capabilities is required to bridge the gap between the expected building energy utilization at the design phase and the actual energy utilization in the building. This difference is known as Energy Performance Gap (EPG). EPG can be up to 5 times the design phase building energy and can have a significant impact on energy efficiencies and climate (Zou et al., 2019). A large portion of the EPG is related to the inability to accurately predict the seasonal performance of the HVAC equipment in a building, which is largely attributed to limitations in equipment models in building simulations ((Imam et al., 2017), (Karlsson et al., 2007)). Major limitations of equipment models are associated with the ability of the model to predict equipment

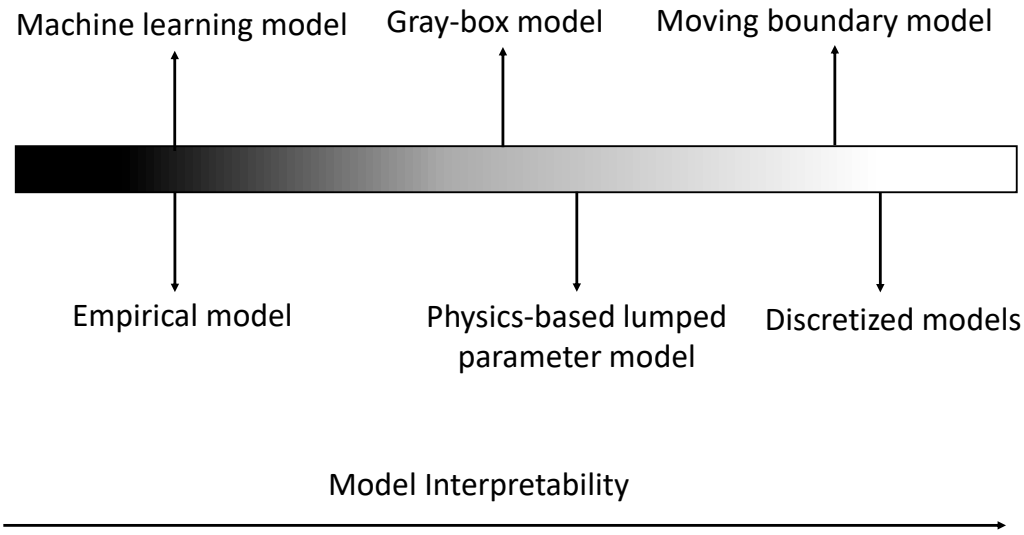

Figure 1: Modeling spectrum with increasing complexity and interpretability.

behaviour accurately across a wide range of operating and load conditions. Modern equipment employs large quantities of discrete control variables to satisfy load throughout the year including variable speed compressors/fans, staging, economizing, and combinations of these variables. These complexities have made existing models of equipment used in building energy modeling ineffective and/or necessitated very large experimental datasets to train them, which is often impractical.

Unitary equipment models fall into two categories on a modeling spectrum, as shown in Figure 1: physics-based (white-box) models and data-driven (black-box) models. White-box models integrate component models through physical laws to formulate system-level models. For instance, heat exchangers (HEX) can be formulated using approaches such as segment-by-segment modeling, moving boundary modeling (MB), or lumping the entire HEX. For example, Rossi (1995), Jiang and Radermacher (2003), Jiang et al. (2006), Bendapudi et al. (2008), and Schalbart and Haberschill (2013) use segment by segment approach while Rasmussen and Alleyne (2006), McKinley and Alleyne (2008), Bendapudi et al. (2008), Bell (2012) and Qiao et al. (2015) use MB methods to name a few. Some studies like Parise (1986), Braun (1988), Jin and Spitler (2002), and Zhang and Canova (2013) *etc* averaged the refrigerant properties over the entire length of HEX by using a single overall heat transfer coefficient time surface area (UA) value. Compressors in white-box models are discretized into one or several control volumes (Qiao et al. (2015), Zhao et al. (2024)) or using mechanistic chamber models (Tanveer et al. (2022), Islam et al. (2023)). The high fidelity of these models results in highly flexible models that do not require large training datasets but have high computational costs. Segment-by-segment models have the highest computational costs followed by MB models. The computational expenses of lumped models are low (Zhang and Canova (2013), Jin and Spitler (2002)) with reasonable accuracy and are used for model order reduction. In general, the physics-based system models are used to draw physical insights by combining individual components and are best suited for system design purposes but are generally too computationally expensive for building energy simulation.

In contrast to the physics-based models, black-box models are created by analyzing data generated by a system under various operating conditions and establishing a statistical relationship between the inputs and outputs through a mathematical function. These models do not require a detailed understanding

of the inner working of the system and are often more accurate in their training envelope with fewer unknowns. However, they tend to have fewer generalization capabilities, meaning they may not perform as well when applied to new or unseen data (Gabel and Bradshaw, 2023). Among these black-box models, empirical models are polynomial equations-based models trained from experimental data for specific model inputs. Yousaf et al. (2024) and Brandemuehl et al. (1993) present empirical models to predict system performance metrics by introducing correction factors to account for the difference in the operational conditions from rated performance. A variant in the black-box category is machine learning (ML) based models. Yousaf et al. (2022), Afram and Janabi-Sharifi (2015), and Zhao et al. (2014) present black-box models that are accurate and fast to respond. The main disadvantages of ML models, besides these being not interpretable, are their poor predictive capabilities beyond training range and the architecture formulation that needs to be optimized on trial and error method (Yousaf et al. (2019) Lu et al. (2021)). These are acceptable in computational efficiency for building energy efficiency but generally fail to capture the seasonal behaviour of a system or require impractically large datasets to do so.

This work proposes a marriage of the extensibility of the physics-based models with the computational efficiency of the black-box models. This marriage is accomplished by developing a model with limited physics that is coupled with regression elements to create a gray-box model. In recent years, considerable research effort has been directed towards the development of hybrid or gray-box formulations, aiming to seamlessly integrate data-driven approaches with physics-based models (Ghattas and Willcox, 2021). The literature review underscores the critical focus on UA in air conditioning and refrigeration system modeling. Notably, several studies employ regression analysis to determine UA, emphasizing its significance in system performance optimization. For instance, Wang et al. (2000) and Jie (2015) base their models on mass flow rates and experimental data, while Jin and Spitler (2002) utilize catalog data to establish a constant UA value. Insights from Liu and Cai (2021) and Leerbeck et al. (2023) highlight UA's pivotal role in fault detection and predictive capabilities in refrigeration systems. Additionally, Hariharan and Rasmussen (2011) and Zsembinszki et al. (2017) contribute to the understanding of UA through their respective investigations on refrigerant mass flow rates and empirical relations. This synthesis of the literature, predominantly focused on chiller-based systems, emphasizes the pivotal role of UA in enhancing air conditioning and refrigeration system performance.

In this paper, we bridge the gap in modeling by presenting a gray-box model for unitary air conditioning equipment, specifically designed to address the EPG. This model is adept at capturing the intricate behaviours of modern equipment using minimal experimental datasets. The key contributions of this work are as follows:

- A novel gray-box steady-state model for unitary equipment that strikes a balance between accuracy and data efficiency, addressing the limitations of both black-box and white-box models.
- Formulated correlations for prediction of UA using genetic algorithm-based symbolic regression.
- Evaluating the predictive performance of the model with fewer training data points demonstrating its robustness and generalization capabilities over experimental data obtained from 3 different units in a wide range of conditions (140 data points).

The development and rigor associated with these contributions are elaborated on in the following sections.

2. Methodology

This section details the gray-box system model, its components, and the methodology for deriving the UA correlations used in heat exchanger simulations. It also explains how these component models are integrated into a comprehensive system model and outlines the data collection methodology employed for model validation.

The gray-box model is a steady-state model that simulates the operation of a Vapor Compression System (VCS). It utilizes fundamental thermodynamics of the VCS, combined with component-specific models to represent the four main components of the cycle and the fans. These component models are developed using a combination of physics-based relationships and data-driven correlations. Notably, the heat exchangers are modeled with an empirical correlation for the UA, derived using a genetic algorithm, which simplifies the information required for model validation. The following sub-sections describe these component models in detail.

2.1. Component models

The main components in the VCS are modeled, the compressor, condenser, evaporator, and expansion device along with indoor and outdoor fans. The state points for these components are shown in Figure 2.

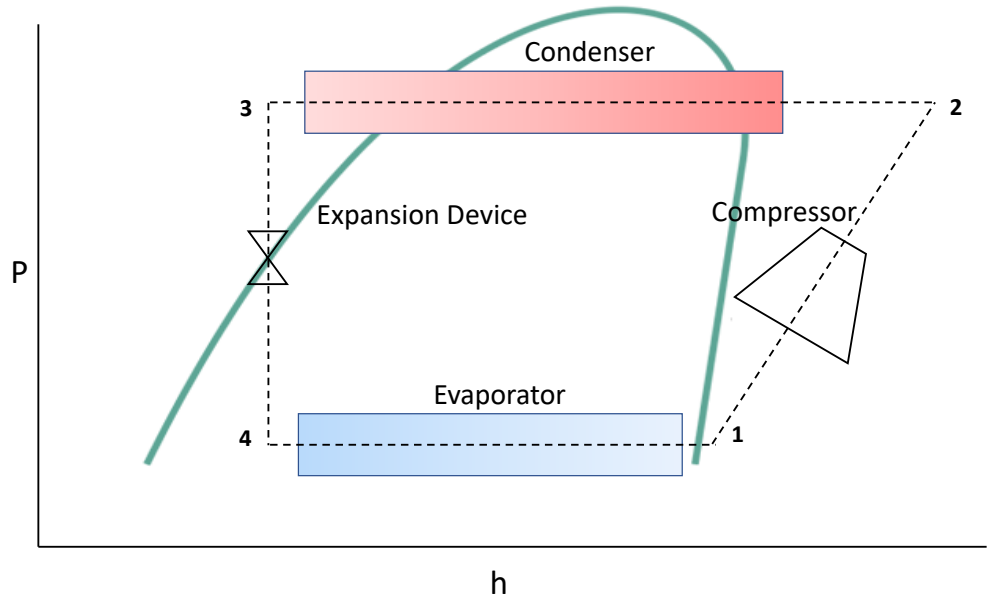

.

Figure 2: State points for each component in gray-box model

2.1.1. Compressor model

The compressor is the heart of the VCS, and its behaviour has a large influence on the overall system-level predictions. Despite their known limitations Gabel and Bradshaw (2023) the AHRI compressor maps are well-known and accepted by the industry and presumably available to nearly all system developers from compressor manufacturers Standard (2020). The AHRI model, also known as the 10-coefficient model, has 3rd-degree polynomial equations for predicting the mass flow rate, power, and capacity of the compressor. These polynomial equations are functions of suction saturation temperature (T_{evap}) and discharge saturation temperatures (T_{cond}) or evaporating (P_{evap}) and condensing pressures (P_{cond}) given as,

$$Y = c_1 + c_2 T_{evap} + c_3 T_{cond} + c_4 {T_{evap}}^2 + c_5 T_{evap} T_{cond} + c_6 {T_{cond}}^2 + c_7 {T_{evap}}^3 + c_8 T_c {T_{evap}}^2 + c_9 T_e {T_{cond}}^2 + c_{10} {T_{cond}}^3, \quad (1)$$

In the equation 1, Y denotes Refrigerating capacity, power Input, or refrigerant mass flow rate while $c_1 ... c_{10}$ are regression coefficients.

These compressor maps are developed at fixed superheat (SH) and subcooling (SC) degrees and require correction if the actual operating superheat or subcooling differs from the mapped quantities. For a different SH at state point 1 in Figure 2, the mass flow rate equation needs to be corrected by the ratio of measured refrigerant density at suction to the standard refrigerant density at the map conditions. Dabiri and Rice (1981) presented a standard correction factor to account for variation in the suction gas SH from the map-based SH to the actual one as,

$$\dot{m}_{ref} = \left[1 + F(\frac{\nu_{map}}{\nu_{act}} - 1)\right] \dot{m}_{ref,map}, \tag{2}$$

where F is 0.75 by default unless provided by the manufacturer. (Dabiri and Rice, 1981) also proposed another correction factor to correct for variance in SH affecting power prediction given as,

$$\dot{W} = \dot{W}_{map} \left(\frac{\dot{m}_{ref}}{\dot{m}_{ref,map}}\right) \frac{\Delta h_{is,act}}{\Delta h_{is,map}}. \tag{3}$$

The enthalpy differences, $\Delta h_{is,act}$ and $\Delta h_{is,map}$, represent the isentropic-actual and isentropic-mapped enthalpy differences, respectively.

The discharge enthalpy, h_2 of the refrigerant is calculated by an energy balance using

$$h_2 = h_{suct} + (1 - f_Q)\frac{\dot{W}}{\dot{m}_{ref}}. \tag{4}$$

If the heat loss (or gain) to the ambient is known along with the compressor power consumption. Generally, it is challenging to predict the compressor shell temperature, and for this reason, it is accepted to use a heat loss factor, (f_Q) value from 10-40% (Chen et al., 2004) given as,

$$f_Q = \frac{\dot{Q}_{loss}}{\dot{W}_{comp}}. \tag{5}$$

2.1.2. Condenser model

Refrigerant from the compressor at state point 2 in Figure 2 is provided to the air-cooled condenser to reject sensible heat and transform the superheated refrigerant into the subcooled high-pressure refrigerant at state point 4. This process is modeled by assuming sensible-only heat rejection (dry air) and a lumped conductance on the refrigerant side. Therefore, it is possible to use the effectiveness-NTU lumped method as given by,

$$\dot{Q}_{cond} = \epsilon_{cond} \dot{m}_{ca} c_{p,a} (T_{cond} - T_{odt}). \tag{6}$$

where,

$$\epsilon_{cond} = 1 - e^{NTU_{cond}}, \tag{7}$$

and

$$NTU_{cond} = \frac{UA_{cond}}{\dot{m_{ca}} c_{pa}}. \tag{8}$$

where the UA_{cond} is the overall conductance of the heat exchanger and is calculated as described in section 2.2. The exit enthalpy of the refrigerant, h_3 from the condenser is calculated as,

$$h_3 = h_2 - \frac{\dot{Q}_{cond}}{\dot{m}_{ref}}. \tag{9}$$

2.1.3. Expansion device model

The purpose of the expansion device is to take advantage of the Joule-Thompson effect of a refrigerant by lowering the pressure from state point 3 to state point 4 and reducing refrigerant temperature below ambient. Expansion devices are categorized as a fixed area such as capillary tubes, and controllable expansion devices such as thermostatic and electronic expansion devices. To model fixed area expansion devices, semi-empirical correlations are recommended to use (Shen, 2006), while to model the controllable expansion devices, SH temperature is provided or mass flow rate across the expansion device is calculated. In the current work, we assume there is some form of active control of the valve such that the SH value is maintained by the system throughout the operation and the valve itself is adiabatic. Therefore the energy balance on the valve reduces to,

$$h_3 = h_4. \tag{10}$$

2.1.4. Evaporator model

Refrigerant from the expansion device enters the evaporator at state point 4. Similar to the condenser, the evaporator is modeled using lumped analysis but, in contrast to the condenser, the analysis assumes a fully wet evaporator where the heat absorption in the evaporator is calculated as,

$$\dot{Q}_{evap} = \epsilon_{evap}\dot{m}_{ea}\left(h_{id}(T_{idt}, T_{iwb}) - h_s(T_{evap}, \phi = 1)\right), \tag{11}$$

where,

$$\epsilon_{evap} = 1 - e^{NTU_{evap}}, \tag{12}$$

and

$$NTU_{evap} = \frac{UA_{evap}}{\dot{m}_{ea}c_{pa}}. \tag{13}$$

Similar to the condenser, the UA_{evap} is calculated using the correlation derived in section 2.2. Additionally, the enthalpy difference is calculated across the evaporator on the air side. The incoming air enthalpy is determined as a function of evaporator air inlet temperature, T_{idt} and indoor wet bulb temperature, T_{iwb} while the supply air enthalpy is determined by neglecting the resistance offered by evaporator tube material and assuming the surface of evaporator temperature equal to the saturation temperature inside evaporator with relative humidity (ϕ) equal to 1.

The bypass factor method (Brandemuehl et al. (1993)) is utilized to calculate the sensible heat ratio (SHR) as,

$$SHR = \frac{h(T_{idt}, \omega_{adp}) - h_{adp}}{h_{id} - h_{adp}}. \tag{14}$$

Where,

$$h_{adp} = h_{id} - \frac{h_{id} - h_{sup}}{1 - BF}. \tag{15}$$

The bypass factor, (BF) represents the amount of air that bypasses the coil and is calculated at the rated conditions (Cheng et al., 2021). It is given as,

$$BF = \frac{h_{sup} - h_{adp}}{h_{id} - h_{adp}}. \tag{16}$$

2.1.5. Fan model

To calculate the power consumed by the fans, fan laws are utilized (ASHRAE, 2020),

$$\dot{W}_{fan} = \frac{\dot{V}}{\dot{V}_{rat}} \dot{W}_{fan,rat}. \tag{17}$$

The fan model requires the rated volumetric flow rate and power consumption. Rated information of the specific unit is used to calculate the fan power consumption at other operating conditions using,

$$\dot{W}_{fan} = \left(a_0 + a_1 \frac{\dot{V}}{\dot{V}_{rat}} + a_2 (\frac{\dot{V}}{\dot{V}_{rat}})^2 \right) \dot{W}_{fan,rat}, \tag{18}$$

where a_0,a_1, and a_2 are coefficients obtained using linear regression using experimental data.

2.1.6. Superheat and subcooling models

The structure of the component-based model presented here requires an input of SH and SC, however, this is atypical for a system model used in BEM simulations and not commonly provided information by unit manufacturers. This is addressed by eliminating SC and SH from the inputs and introducing submodels for the prediction of SH and SC. The SH submodel uses SH value at the rated conditions as an initial input and is corrected for differences in the actual conditions to the rated conditions through a correction factor for all other indoor and outdoor operational conditions,

$$SH = \left(\frac{T_{odt}.T_{iwb,rat}}{T_{odt,rat}.T_{iwb}} \right) * SH_{rat}. \tag{19}$$

A submodel for the estimation of SC temperature is developed that uses a first-degree polynomial equation with SH temperature as,

$$SC = \alpha_0 + \alpha_1 * SH. \tag{20}$$

The coefficients α_0 and α_1 are to be updated using linear regression analysis from experimental data.

2.2. Derivation of heat exchanger UA correlations using genetic algorithms

The physics-based heat exchange component models described in the previous section use the UA to determine the heat exchanger's effectiveness. The UA is calculated as,

$$UA = \frac{1}{\frac{1}{A_a h_a} + \frac{1}{A_{ref} h_{ref}}}, \tag{21}$$

where A_a and A_{ref} are the surface areas of the air and refrigerant side of the coils, respectively, and h_a and h_{ref} are the average heat transfer coefficients of the air and refrigerant side of the coils, respectively. The heat transfer coefficients of air and refrigerant sides are calculated using correlations which are a function of the geometry of the heat exchanger. These geometric details of the heat exchangers are hard to find/calculate and are often known to manufacturers only, making estimating these based on Equation 21 impractical. The current work proposes a correlation to calculate the UA for the evaporator and condenser in terms of the air-side inputs to the model.

2.2.1. Formulation of UA correlations

Both UA correlations for the evaporator and condenser are developed in a two-step process, the first step is the identification of the most critical input parameters, and the second step is using the identified inputs to develop the functional form for the correlation. Finally, the non-linear least square method uses experimental data to fit a correlation.

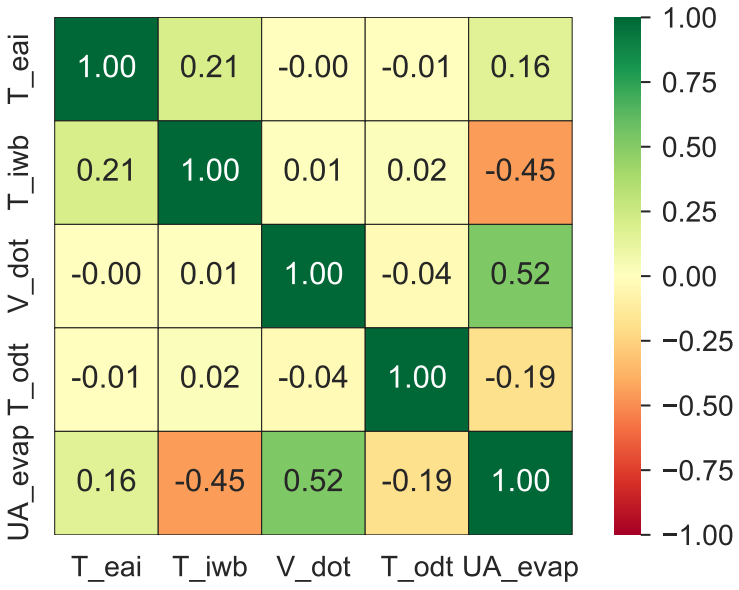

Figure 3: Pearson correlation matrix for evaporator UA

To identify the most critical inputs for the UA correlation, Pearson's correlation matrix (Rodgers and Nicewander, 1988) is obtained as shown in Figure 3 for the evaporator. There is positive correlation of T_{eai} and $\dot{V}$ and negative correlation of T_{iwb} and T_{odt} with UA for evaporator for these variables. Based on this relationship, UA for the evaporator is a function of the variables available to model input as,

$$UA_{evap} = f(T_{eai}, \dot{V}, T_{iwb}, T_{odt}). \tag{22}$$

This process is repeated for the condenser and it is discovered that it is a function of the condenser air inlet temperature (T_{odt}) only,

$$UA_{cond} = f(T_{odt}). \tag{23}$$

Once the most appropriate input variables are identified a final correlation formulation is generated using genetic algorithm-based Symbolic Regression (SR). SR is a method that uses evolutionary computation to find mathematical equations that can explain the relationship between input and output data (Cranmer, 2023*a*). Unlike traditional regression techniques which only find the best values for the parameters of a pre-defined equation, SR uses evolutionary algorithms to search for the best equation that fits the data. The algorithm explore different combinations of mathematical operators and operands to find the equation that minimizes the error between the predicted and actual results. SR, in the literature, is used to discover the hidden physics from data (Vaddireddy et al., 2020) as well as the development of an optimized energy management system (Kefer et al., 2022). These algorithms are been coded into a Python package available at Cranmer (2023*b*), which are utilized for this work. The final correlation obtained through the use of SR for evaporator is shown as following,

$$UA_{evap} = -\frac{(T_{odt} - T_{iwb})^3}{T_{odt}} + e_0\sqrt{\dot{V}} - e_1\dot{V}\left((T_{iwb} - T_{idt})^3 - T_{odt} + e_4.\dot{V}\frac{e_2}{e_3 - \dot{V}}\right), \tag{24}$$

where e_0, e_1..e_4 are regression coefficients. Temperatures, T_{odt}, T_{iwb}, and T_{idt} are in K. At the same time, flowrate, $\dot{V}$, is in the units of m^3s^{-1} and UA_{evap} would be in WK^{-1}. It should be noted that this format does not closely align with any known physical laws or relationships and is instead purely empirical. This was concerning to the authors and was critically analysed. The correlation was benchmarked against a

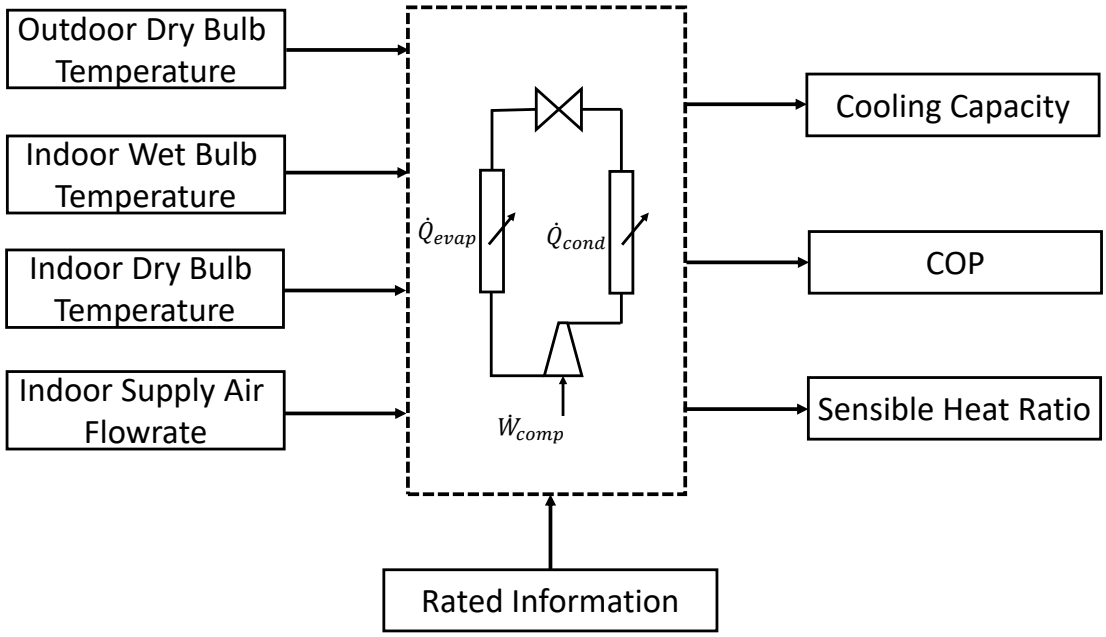

Figure 4: System model inputs and outputs.

heuristically derived one. The SR-derived correlation demonstrated superior performance, which justified its inclusion in this work.

The UA for the condenser is notably less complex compared to that of the evaporator across the three units and as such did not warrant the use of SR. Since the outdoor unit primarily responds to outdoor temperature fluctuations, a heuristically derived empirical correlation is expressed as an affine function of T_{odt}-measured in K,

$$UA_{cond} = (c_0 + c_1 T_{odt}) UA_{cond,rat}, \tag{25}$$

where c_0, c_1 are regression coefficients for condenser UA correction factor, and $UA_{cond,rat}$ is condenser UA at rated conditions which is measured in WK^{-1}.

2.3. System model

The overarching goal of the system model is to include the same, or very similar, input parameters as typical system models used in BEM, using the component models developed in the previous section. For models used in BEM, a system operating in cooling mode, requires three input temperatures the outdoor dry bulb (T_{odt}), indoor dry bulb (T_{eai}), and indoor wet bulb (T_{iwb}) temperatures. Additionally, the indoor fan air supply, $\dot{V}$ is also assumed to be known. These four model inputs are recommended for formulation of a quasi-steady state system model after investigation of numerous candidate inputs from experimental data obtained from unitary equipment as mentioned in Yousaf et al. (2023). On top of the four input parameters, the rated information about the unit is also required, as shown in Figure 4, including the rated cooling capacity, sensible capacity, indoor and outdoor fan power, supply air for indoor and outdoor fans, and superheat temperature which is readily available information from the unit manufacturer.

The major outputs of the model are compressor power ($\dot{W}$), indoor fan power ($\dot{W}_{fan}$), evaporator cooling capacity $\dot{Q}_{evap}$, condenser heat rejection capacity $\dot{Q}_{cond}$, sensible heat ratio (SHR), and COP. Among these, the performance metrics selected for evaluation are cooling capacity, COP, and SHR as shown in Figure 4.

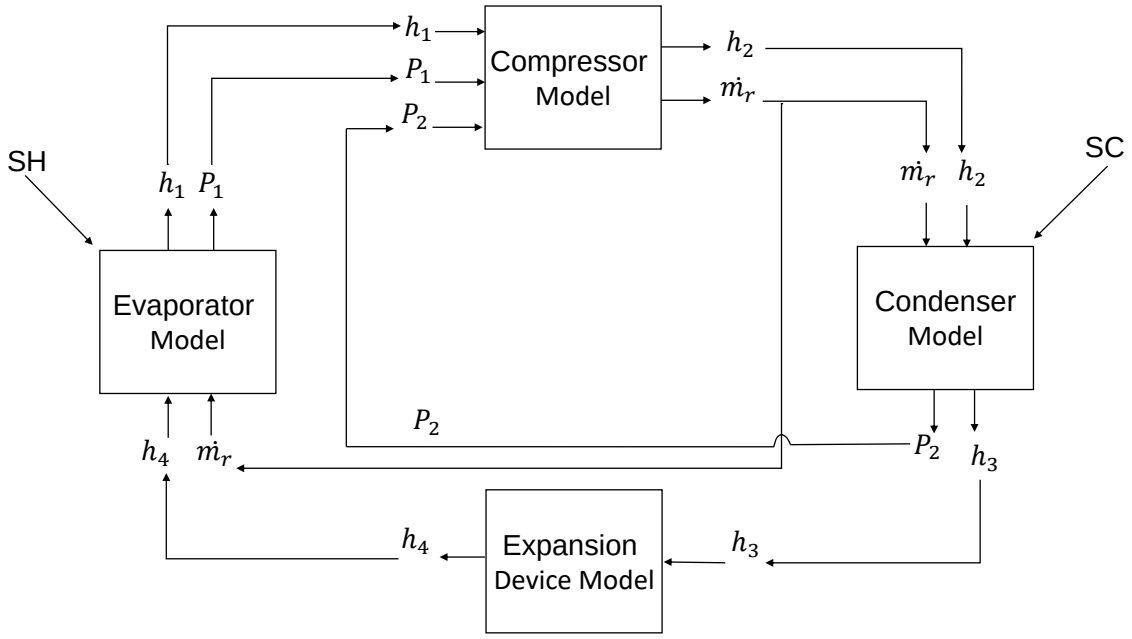

Figure 5: Component model integration into system model.

All the component models are integrated and a system model is formulated as shown in Figure 5. The resulting system model is therefore reflective of the underlying assumptions made by each of the component models, summarized as:

- Steady-state operation with negligible changes in kinetic and potential energies.
- Pressure drop in the heat exchangers is neglected.
- Heat exchangers function in a counter-flow configuration.

Component models are formulated to iterate on the evaporator saturation temperature T_{evap} and condenser saturation temperature T_{cond}, while being constrained by conservation of energy for the VCS given as:

$$\dot{W}_{comp} - \dot{Q}_{loss} + \dot{Q}_{evap} - \dot{Q}_{cond} = 0. \tag{26}$$

The final values of T_{evap} and T_{cond}, are calculated from a residual calculation based on the above constraint. The first residual, defined to obtain the value of T_{evap}, is formulated based on the entry of the compressor and exit of the evaporator as,

$$Residual_1 = \dot{m}_{ref}(h_1 - \overline{h}_1), \tag{27}$$

where h_1 is the enthalpy calculated based on T_{evap} at the current iteration and $\bar{h}_1$ is the enthalpy calculated based on the energy balance constraint. The second residual formulated based on the entry of the condenser and exit of the compressor to obtain T_{cond} as,

$$Residual_2 = \dot{m}_{ref}(h_2 - \overline{h}_2), \tag{28}$$

where h_2 is the enthalpy calculated based on T_{cond} at the current iteration and $\bar{h}_2$ is the enthalpy calculated based on the energy balance constraint. The nonlinear solver *fsolve* from SciPy (Virtanen et al., 2020) is used to solve for the unknowns and drive these residuals to zero. Once, the two residuals converge satisfying the energy conservation across the system, Equation 11 is used to calculate the cooling capacity,

SHR of the system is calculated using Equation 14, and the COP is calculated as

$$COP = \frac{\dot{Q}_{evap}}{\dot{W}_{Net}}, \tag{29}$$

where $\dot{W}_{Net}$ is the combined work consumed by the compressor and indoor and outdoor fans.

2.4. Unitary equipment data collection for model validation

To evaluate the gray-box model performance, unitary equipment data is obtained from three AC systems of capacity 12.3 (3.5), 14 (4), and 17.6 (5) kW (Tons) cooling capacity. High-fidelity data is recorded for varying conditions of outdoor temperatures, indoor temperatures, and airflow conditions along with the compressor speed utilizing a pair of psychrometric chambers. The outdoor temperature is varied from 12.7 ^{o}C (55 ^{o}F) to 51.67 ^{o}C (125 ^{o}F) for all three units. The air handling unit, placed in the indoor room, is exposed to dry bulb temperatures of 23.9 ^{o}C (75 ^{o}F) and 26.6 ^{o}C (80 ^{o}F) with wet bulb temperatures varying from 13.9 ^{o}C (57 ^{o}F) to 22.2 ^{o}C (72 ^{o}F). Different combinations of fan speed and compressor speed are utilised to run the unit at different part load conditions of operation. The resulting test matrices include a total of 140 data points recorded in compliance with ASHRAE 37. A schematic of the experimental AC system test setup showing key sensors in the psychrometeric chamber is shown in Figure 6. More details about the variation in operational inputs are listed in Table 1.

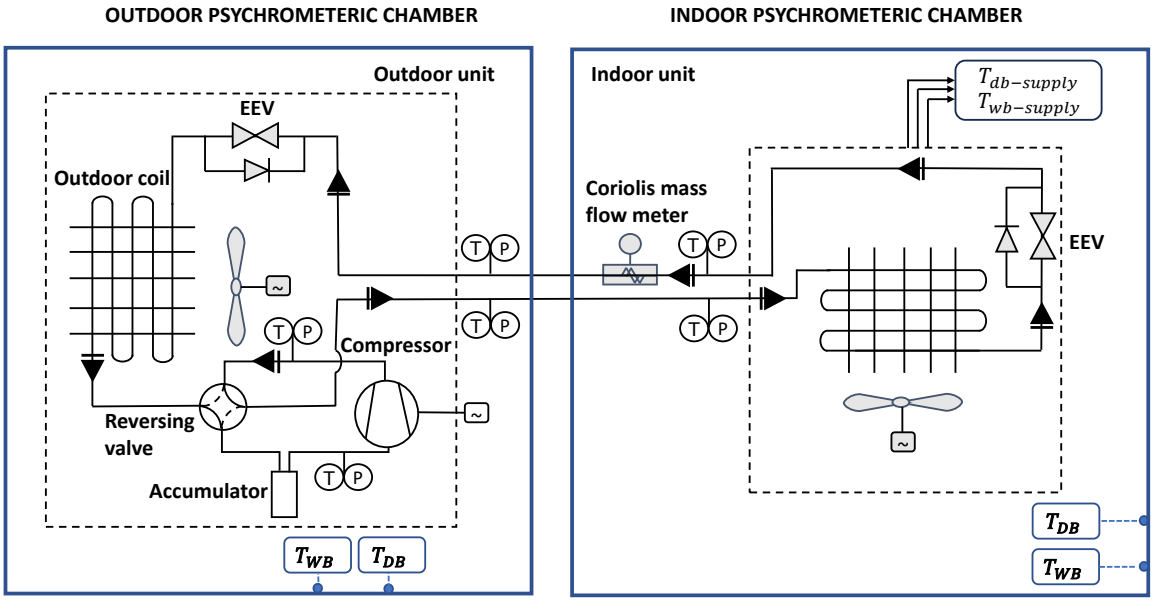

Figure 6: Schematic showing locations of key sensors in the unitary equipment.

Table 1: Unitary equipment experimental-data description.

Field	Unit-1	Unit-2	Unit-3	Measurement Unit
Equipment capacity	12.3 (3.5)	14.0 (4)	17.6 (5)	kW (Tons)
T_{odt} **range**	12.77-51.67 (55-125)	12.77-51.67 (55-125)	12.77-51.67 (55-125)	°C (°F)
T_{iwb} **range**	13.9-22.22 (57-72)	13.9-22.22 (57-72)	13.9-22.22 (57-72)	°C (°F)
T_{eai} **range**	23.9-26.7 (75-80)	23.9-26.7 (75-80)	23.9-26.7 (75-80)	°C (°F)
$\dot{V}$ **range**	0.42-0.825 (890-1750)	0.53-0.85 (1130-1800)	0.71-0.94 (1500-2000)	m^3/s (CFM)
Compressor speed	HI -Low	HI -Low	HI	-
Total data points	50	40	50	-

2.4.1. Uncertainty analysis

This section reports the systematic uncertainty of all the instruments utilized in the experiments. Additionally, propagated uncertainty is estimated using the method proposed by Taylor et al. (1994) for cooling capacity.

System cooling capacity is determined using enthalpy difference across both sides of the evaporator on the air side as a function of volumetric air flow rate. Details about the kind of sensors used to collect data are provided in Table 2. The relative uncertainty of several of the measurements (*e.g.* pressure) varies based on operating condition, resulting in variable propagated uncertainty of capacity. Table 3 reports the resulting ranges of uncertainties associated with cooling capacity. For the power consumption, the maximum uncertainty associated is 12 W.

Table 2: Sensor accuracy and usage for data collection.

Sensor	**Accuracy**	**Use**
Thermocouples	0.5 °C (0.9 °F)	Air side temperature
Pressure sensor	±0.06% of F.S	Refrigerant side pressure
Power meter	±0.1% of F.S	Indoor and outdoor unit power
Coriolis flow meter	±0.1% of rate	Refrigerant flow rate
Dew point hygrometer	0.15 °C (±.27 °F)	Dew point

Table 3: Range of airside uncertainty associated with cooling capacity.

Unit	**Minimum [kW (Ton)]**	**Maximum [kW (Ton)]**
Unit-1	0.32 (0.10)	0.72 (0.20)
Unit-2	0.38 (0.11)	0.75 (0.21)
Unit-3	0.46 (0.13)	0.83 (0.23)

2.4.2. Model evaluation using experimental data

Using the data generated the models predictive capabilities are evaluated using two error metrics, mean absolute percentage error (MAPE) and root mean square error (RMSE). MAPE measures the average absolute percentage difference between the predicted and actual values, while RMSE measures the average squared difference between the predicted and actual values, and then takes the square root of the results. MAPE and RMSE are given as in Equation 30 and Equation 31 respectively.

$$MAPE = \frac{100}{n} \sum_{i=1}^{n} \frac{|y_i - \hat{y}_i|}{y_i}, \tag{30}$$

$$RMSE = \sqrt{\frac{1}{n} \sum_{i=1}^{n} (y_i - \hat{y}_i)^2}. \tag{31}$$

where 'n' is the number of data points, 'y_i' is the actual value, and '$\hat{y}_i$' is the predicted value.

MAPE is particularly useful when comparing models with varying magnitudes, as it provides a percentage-based error metric, which can be easier to interpret. On the other hand, RMSE is a metric that is sensitive to larger errors, which makes it easier to identify when a model is performing poorly.

3. Results and discussion

In this section, the component-based gray-box model developed in the previous section is used to predict experimental data, and the error in those predictions is analyzed. This analysis begins with an evaluation of the predictive capabilities of the UA sub-models developed in Section 2.2, culminating in SR derived UA for the evaporator presented in Equation 24 and the heuristically derived UA for the condenser presented in Equation 25. Finally, the complete system model predictions are evaluated against experimental data, and trends in error are discussed and analyzed.

3.1. UA correlation training and validation

Each UA formulation is evaluated for robustness by training the correlations with 100% of the data collected and 10% of the total data, which is 5 data points for each unit. The results are compared against the UA from the experiment, which represents the UA needed to satisfy Equations 11 to 13 for the evaporator and Equations 6 to 8 for the condenser, given the experimentally obtained state points and capacities.

Figure 7 shows the performance of both correlations in the 100% and 10% (5 data point) training scenarios. It is noted that both correlations provide better predictive capabilities when trained with the complete dataset (10.66% vs, 14.25% MAPE for the evaporator and 2.60% vs, 8.88% MAPE for the condenser) but it is discovered that this level of improvement did not provide a demonstrable impact on the gray-box model's overall predictive capability. Therefore, the 10% training methodology is employed for the UA training, using the same data points used to train the gray-box model. The authors believe it is important to detail the criteria used for selecting training points in this work. The training points are chosen to represent the full operational envelope. Specifically, two extreme points (high and low temperatures), one at the rated temperature, and two additional points on either side of the rated temperature are selected to train the model effectively.

3.2. Gray-box model results

All the component models are integrated to comprise the system model which is evaluated on an experimental data set for the three units in a low training data scenario. The model is trained with 5 data points and tested on the remaining data. Figure 8a shows the MAPE for the performance metrics of three heat pump systems. The model predicts all three performance metrics of cooling capacity, COP, and SHR within a reasonable MAPE range of less than 3.2%. Figure 8a suggests that the model is more accurate on Unit-3, Unit-1, and Unit-2, respectively. The average heat balance in the experimental data for the air-side and refrigerant side in Unit-1, Unit-2, and Unit-3 is 2.75%, 6.99%, and 1.65%, which is consistent with the model error trend across the three units. Similarly, the other error metric used for model evaluation purposes is the RMSE and Figure 8b shows the RMSE for the performance metrics of all units. The model is observed to be predicting cooling capacities, COP, and SHR with consistent predictive capabilities indicating model stability and reliability. Figure 9 shows parity plots for Unit-1 for prediction of cooling capacity, COP, and SHR. The parity plots show that the cooling capacity is estimated within a range of $\pm$ 7.5%, the COP is predicted in a range of -7.5% to +5% whereas the SHR for the same unit is in the range of -2% to +5%. These parity plots show that the model predictions are evenly distributed above and below the parity line, showcasing the model's unbiased behavior towards overestimation or underestimation. This balance prediction enhances the model reliability and trustworthiness in as few as 10% (only 5) training data points from the operational envelope of the unitary AC system. Similar behaviour is observed for the other two units examined as well.

The gray-box model results for the three units in different cases demonstrate its ability to accurately predict performance metrics even when trained on a limited data set with as low as 5 data points.

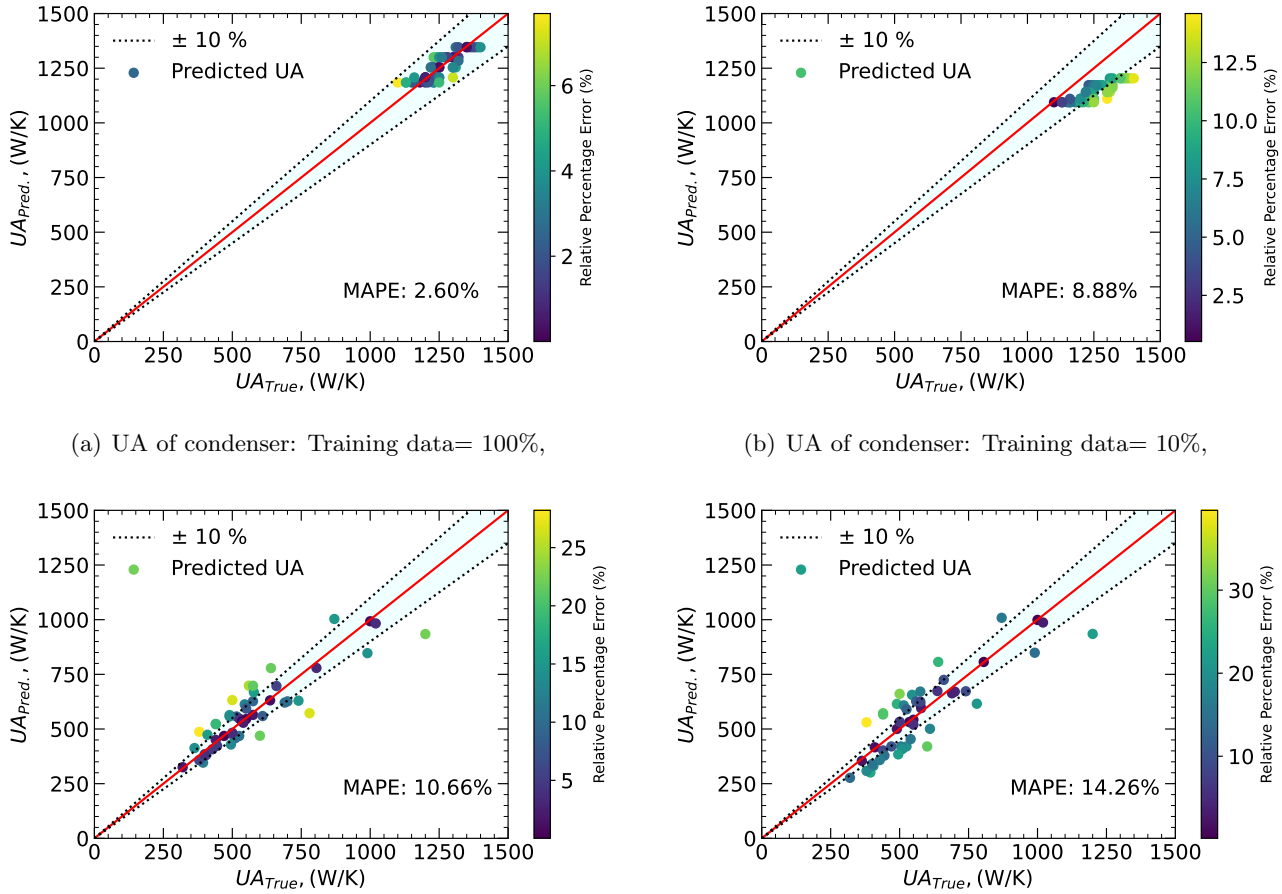

(a) UA of condenser: Training data= 100%,

(b) UA of condenser: Training data= 10%,

(c) Symbolic regression: Training data= 100%,

(d) Symbolic regression: Training data= 10%,

Figure 7: Predictive performance of the two UA correlations on 100% and 10% training data.

4. Conclusions

The modeling of unitary AC systems presents considerable challenges. Existing white-box methods exhibit a trade-off between accuracy and computational cost, while black-box models lack the level of trustworthiness required by industry standards. There is a critical need for algorithms that offer both efficiency and accuracy, along with effective integration with sparse observations. In this study, we aimed to introduce a gray-box model for unitary air conditioning equipment that demonstrates the ability to achieve accuracy with minimal data points, utilizes standard inputs for building energy simulation, and offers reliable performance.

To this end, the proposed gray-box model for unitary air conditioning equipment offers a simplified solution to overcome the limitations of both black-box and white-box models. By utilizing a component-based approach and a genetic algorithm to formulate the correlation of the overall heat transfer coefficient, the model achieved satisfactory accuracy in predicting the cooling capacity, COP, and SHR of three state-of-the-art air conditioning systems. The final model can predict 140 experimental data points across three different sizes of unitary air-conditioners with MAPE's of 3.20% or less for cooling capacity, COP and SHR for all units. In the process some conclusions can be drawn as follows:

- The correlation formulated through the use of a symbolic regression generated UA predictions for the evaporator that are sufficient for very good predictive capabilities of the gray-box model.

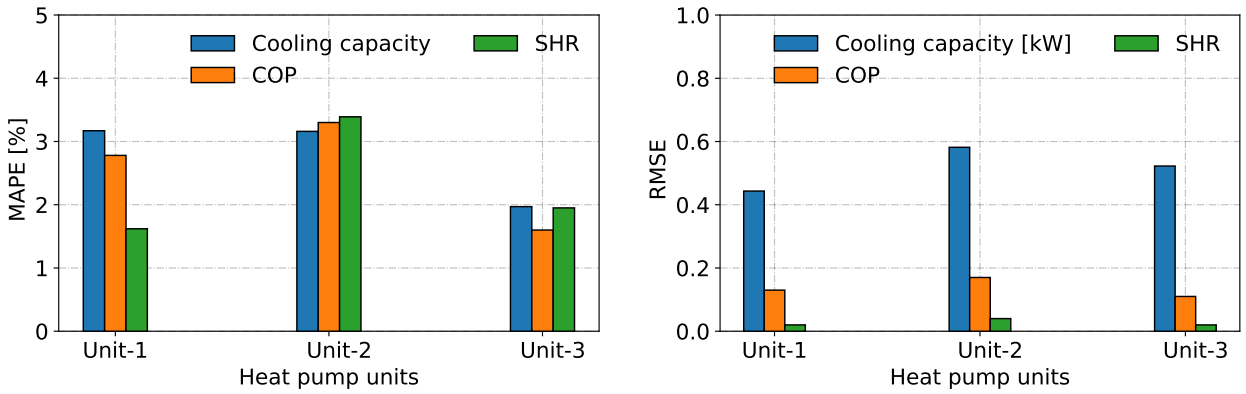

(a) MAPE

(b) RMSE

Figure 8: MAPE and RMSE of model for 3 heat pump units in AC mode operation.

- The model provides consistent results and offers low training data requirements (5 data points) highlighting the robustness of the model, making it a valuable tool for air conditioning performance prediction and building energy optimization.
- The model relies solely on operational inputs and ambient temperatures, making it compatible with existing BEMs.

The gray-box model developed in this study presents a promising solution for energy management and optimization in air conditioning systems since it is compatible with existing BEMs. Its accuracy makes it a valuable tool for building energy optimization and reducing energy consumption. However, the model also has some limitations. The model's performance can be impacted by the quality of the training data (adherence to ASHRAE standards in data collection), thereby affecting its overall effectiveness. Furthermore, the model is not evaluated on the heating operation and its effectiveness can be explored in the future. Despite these limitations, the gray-box model offers a promising approach for a more sustainable future, and further research can be done to improve its performance and applicability, particularly the selection of training data.

Acknowledgement

This research was supported by the Oklahoma Center for the Advancement of Science and Technology (OCAST) with grant number AR-042, and by the Center for Integrated Buildings Systems (CIBS), an Industry/University Cooperative Research Center at Oklahoma State University.

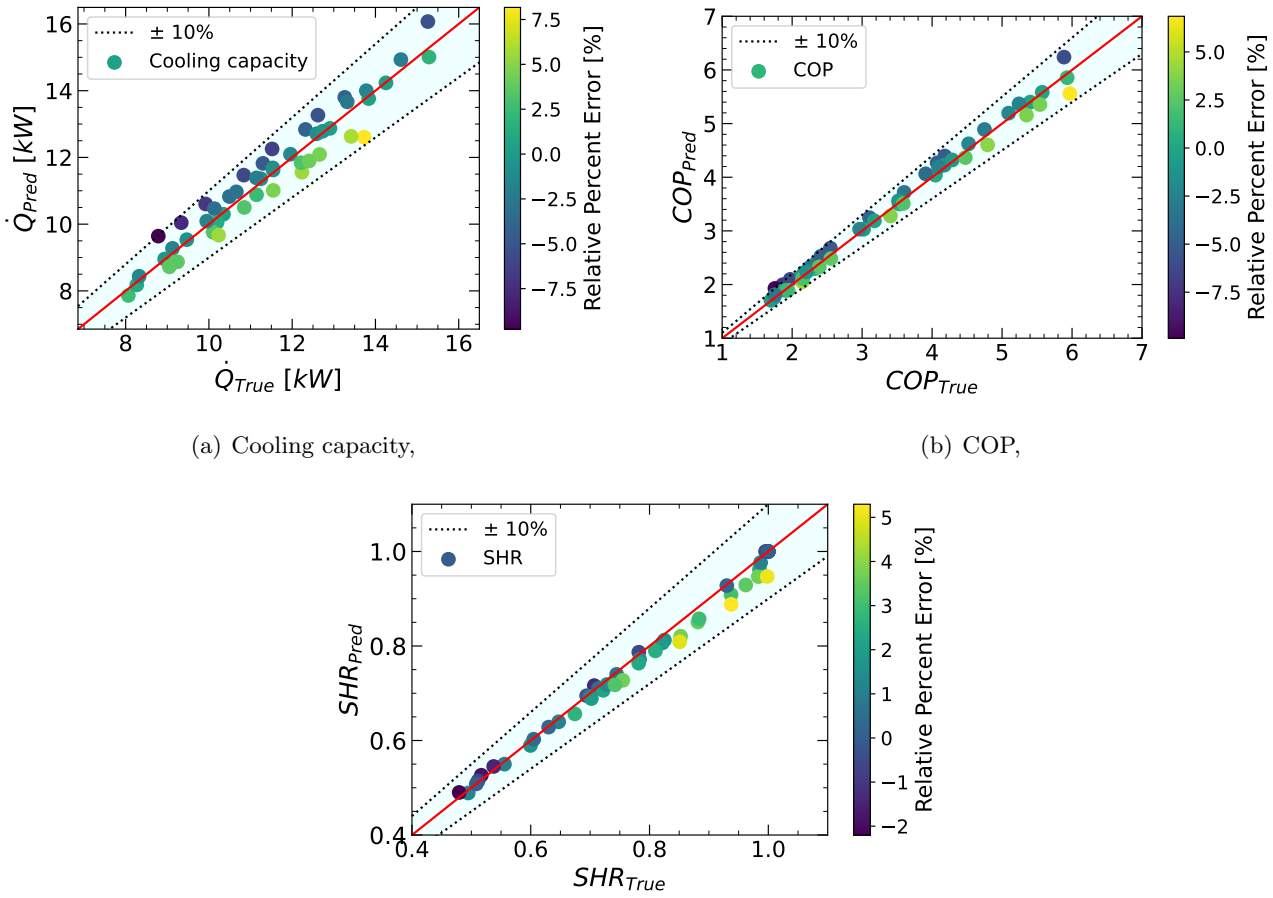

(a) Cooling capacity,

(b) COP,

(c) SHR.

Figure 9: Representative parity plots for Unit-1

References

AEO (2020), 'Annual energy outlook 2020', *Energy Information Administration, Washington, DC* **12**, 1672–1679.

Afram, A. and Janabi-Sharifi, F. (2015), 'Black-box modeling of residential hvac system and comparison of gray-box and black-box modeling methods', *Energy and Buildings* **94**, 121–149.

ASHRAE (2020), 'Ashrae fundamentals handbook'.

Bell, I. (2012), 'ACHP', `https://achp.sourceforge.net/`.

Bendapudi, S., Braun, J. E. and Groll, E. A. (2008), 'A comparison of moving-boundary and finite-volume formulations for transients in centrifugal chillers', *International journal of refrigeration* **31**(8), 1437–1452.

Brandemuehl, M., Gabel, S. and Andresen, I. (1993), 'Hvac 2 toolkit: Algorithms and subroutines for secondary hvac system energy calculations. atlanta: American society of heating, refrigerating and air-conditioning engineers'.

Braun, J. E. (1988), *Methodologies for the design and control of central cooling plants*, The University of Wisconsin-Madison.

Chen, Y., Braun, J. E. and Groll, E. A. (2004), 'Modeling of hermetic scroll compressors: model development', *HVAC&R Research* **10**(2), 129–152.

Cheng, L., Braun, J. E. and Horton, W. T. (2021), 'A methodology for mapping the performance of variable-speed residential cooling equipment using load-based testing', *International Journal of Refrigeration* **132**, 133–144.

Cranmer, M. (2023*a*), 'Interpretable machine learning for science with pysr and symbolicregression. jl', *arXiv preprint arXiv:2305.01582* .

Cranmer, M. (2023*b*), 'Pysr', `https://astroautomata.com/PySR//`.

Dabiri, A. and Rice, C. (1981), 'A compressor simulation model with corrections for the level of suction gas superheat', *Ashrae Transactions* **87**(Part 2), 771–782.

Gabel, K. S. and Bradshaw, C. R. (2023), 'Evaluation and quantification of compressor model predictive capabilities under modulation and extrapolation scenarios', *International Journal of Refrigeration* **149**, 1–10.

Ghattas, O. and Willcox, K. (2021), 'Learning physics-based models from data: perspectives from inverse problems and model reduction', *Acta Numerica* **30**, 445–554.

Hariharan, N. and Rasmussen, B. P. (2011), 'Parameter estimation of dynamic vapor compression system models using limited sensor information', *ASHRAE Transactions* **117**(2), 746–759.

Imam, S., Coley, D. A. and Walker, I. (2017), 'The building performance gap: Are modellers literate?', *Building Services Engineering Research and Technology* **38**(3), 351–375.

Islam, M., Nicholas, J. and Bradshaw, C. R. (2023), 'Development and experimental validation of a mechanistic chamber model of a novel peristaltic compressor', *International Journal of Refrigeration* **146**, 430–441.

Jiang, H., Aute, V. and Radermacher, R. (2006), 'Coildesigner: a general-purpose simulation and design tool for air-to-refrigerant heat exchangers', *International Journal of Refrigeration* **29**(4), 601–610.

Jiang, H. and Radermacher, R. (2003), 'A distributed model of a space heat pump under transient conditions', *International journal of energy research* **27**(2), 145–160.

Jie, C. (2015), 'Gray-box modeling of multistage direct-expansion units to enable control system optimization', *ASHRAE Transactions* **121**, 203.

Jin, H. and Spitler, J. D. (2002), 'A parameter estimation based model of water-to-water heat pumps for use in energy calculation programs', *ASHRAE transactions* **108**, 3.

Karlsson, F., Rohdin, P. and Persson, M.-L. (2007), 'Measured and predicted energy demand of a low energy building: important aspects when using building energy simulation', *Building Services Engineering Research and Technology* **28**(3), 223–235.

Kefer, K., Hanghofer, R., Kefer, P., Stöger, M., Hofer, B., Affenzeller, M. and Winkler, S. (2022), 'Simulation-based optimization of residential energy flows using white box modeling by genetic programming', *Energy and Buildings* **258**, 111829.

Leerbeck, K., Bacher, P., Heerup, C. and Madsen, H. (2023), 'Grey box modeling of supermarket refrigeration cabinets', *Energy and AI* **11**, 100211.

Liu, H. and Cai, J. (2021), 'A robust gray-box modeling methodology for variable-speed direct-expansion systems with limited training data', *International Journal of Refrigeration* **129**, 128–138.

Lu, C., Li, S. and Lu, Z. (2021), 'Building energy prediction using artificial neural networks: A literature survey', *Energy and Buildings* p. 111718.

McKinley, T. L. and Alleyne, A. G. (2008), 'An advanced nonlinear switched heat exchanger model for vapor compression cycles using the moving-boundary method', *International Journal of refrigeration* **31**(7), 1253–1264.

Parise, J. A. (1986), 'Simulation of vapour-compression heat pumps', *Simulation* **46**(2), 71–76.

Qiao, H., Aute, V. and Radermacher, R. (2015), 'Transient modeling of a flash tank vapor injection heat pump system–part i: Model development', *International journal of refrigeration* **49**, 169–182.

Rasmussen, B. P. and Alleyne, A. G. (2006), Dynamic modeling and advanced control of air conditioning and refrigeration systems, Technical report, Air Conditioning and Refrigeration Center. College of Engineering ....

Rodgers, J. L. and Nicewander, W. A. (1988), 'Thirteen ways to look at the correlation coefficient', *The American Statistician* **42**(1), 59–66.

Rossi, T. M. (1995), Detection, diagnosis, and evaluation of faults in vapor compression equipment, PhD thesis, Purdue University.

Schalbart, P. and Haberschill, P. (2013), 'Simulation of the behaviour of a centrifugal chiller during quick start-up', *International journal of refrigeration* **36**(1), 222–236.

Shen, B. (2006), Improvement and validation of unitary air conditioner and heat pump simulation models at off-design conditions, PhD thesis, Purdue University.

Standard, A. (2020), 'Performance rating of positive displacement refrigerant compressors and compressor units'.

Tanveer, M. M., Bradshaw, C. R., Ding, X. and Ziviani, D. (2022), 'Mechanistic chamber models: A review of geometry, mass flow, valve, and heat transfer sub-models', *International Journal of Refrigeration* **142**, 111–126.

Taylor, B. N., Kuyatt, C. E. et al. (1994), *Guidelines for evaluating and expressing the uncertainty of NIST measurement results*, Vol. 1297, US Department of Commerce, Technology Administration, National Institute of Standards and Technology.

Vaddireddy, H., Rasheed, A., Staples, A. E. and San, O. (2020), 'Feature engineering and symbolic regression methods for detecting hidden physics from sparse sensor observation data', *Physics of Fluids* **32**(1), 015113.

Virtanen, P., Gommers, R., Oliphant, T. E., Haberland, M., Reddy, T., Cournapeau, D., Burovski, E., Peterson, P., Weckesser, W., Bright, J. et al. (2020), 'Scipy 1.0: fundamental algorithms for scientific computing in python', *Nature methods* **17**(3), 261–272.

Wang, S.-w., Wang, J. and Burnett, J. (2000), 'Mechanistic model of centrifugal chillers for hvac system dynamics simulation', *Building services engineering research and technology* **21**(2), 73–83.

Yousaf, S., Bradshaw, C., Kamalapurkar, R. and San, O. (2022), 'Physics informed machine learning based reduced order model of unitary equipment', *19th International Refrigeration and Air Conditioning Conference* .

Yousaf, S., Bradshaw, C., Kamalapurkar, R. and San, O. (2024), 'Development and performance evaluation of black-box models for air-conditioners and heat pumps at part load operation', *Science and Technology for the Built Environment* .

Yousaf, S., Bradshaw, C. R., Kamalapurkar, R. and San, O. (2023), 'Investigating critical model input features for unitary air conditioning equipment', *Energy and Buildings* p. 112823.

Yousaf, S., Shafi, I., Din, S., Paul, A. and Ahmad, J. (2019), 'A big data analytical framework for analyzing solar energy receptors using evolutionary computing approach', *Journal of Ambient Intelligence and Humanized Computing* **10**(10), 4071–4083.

Zhang, Q. and Canova, M. (2013), Lumped-parameter modeling of an automotive air conditioning system for energy optimization and management, *in* 'Dynamic Systems and Control Conference', Vol. 56123, American Society of Mechanical Engineers, p. V001T04A003.

Zhao, L., Cai, W.-J. and Man, Z.-H. (2014), 'Neural modeling of vapor compression refrigeration cycle with extreme learning machine', *Neurocomputing* **128**, 242–248.

Zhao, Y., Du, Y., Lin, J., Guo, N. and Wu, J. (2024), 'Start-up characteristics of a r290 rotary compressor for an air source heat pump under low ambient temperature condition', *International Journal of Refrigeration* **159**, 385–394.

Zou, P. X., Wagle, D. and Alam, M. (2019), 'Strategies for minimizing building energy performance gaps between the design intend and the reality', *Energy and buildings* **191**, 31–41.

Zsembinszki, G., de Gracia, A., Moreno, P., Rovira, R., González, M. Á. and Cabeza, L. F. (2017), 'A novel numerical methodology for modelling simple vapour compression refrigeration system', *Applied Thermal Engineering* **115**, 188–200.

Appendix A. Gray-box Model Coefficients and input data for Unit-1

This section provides compressor map coefficients from the manufacturer for refrigerant mass flow rate (lb/hr) and power consumption (W). Additionally, regression coefficients for the UA of the evaporator and condenser are listed along with the indoor fan coefficients for power prediction. Rated information of Unit-1 is also provided.

Table A1: Model inputs and coefficients for Unit-1

Coefficient	**1**	**2**	**3**	**4**	**5**	**6**	**7**	**8**	**9**	**10**
Refrigerant mass flowrate, (lb/hr)	378.134	5.50221	-4.04482	0.042809	-0.00535	0.0401347	0.000155	-5.9E-07	1.88E-05	-0.00014
Power consumption in compressor, (W)	689.645	6.58453	9.84749	0.050167	-0.14283	5.33778E-05	-0.00076	-0.00026	0.000732	0.000666
UA for evaporator, (W/K)	560.829095	0.498174156	-0.36116	0.826038	12.07165					
Indoor fan power coefficients, (W)	3.086632017	-7.18860259	5.094972							
Condenser UA coefficients, c (W/K)	2.00579905	-0.00345089								
Refrigerant	R410A									
Heat lost to ambient, (%)	20									
Displacement scale factor, (-)	1									
Outdoor fan volumetric flow rate, (m^3/s)	2									
Atmospheric pressure (Pa)	98200									
Outdoor fan power, (W)	210									
Rated UA for condenser, (W/K)	1920									
Rated indoor fan volumetric flow rate	0.8226									
Rated power of indoor fan, (W)	636									
Rated total cooling capacity, (W)	12907									
Rated sensible capacity, (W)	10068									